Int. J. Heat Mass Transfer. Vol. 35, No. 9, pp. 2203–2218, 1992
Printed in Great Britain

0017–9310/92 $5.00 + 0.00

Reflux condensation phenomena in single vertical tubes

R. GIRARD† and J. S. CHANG
Department of Engineering Physics, McMaster University, Hamilton, Ontario, L8S 4M1, Canada

(*Received* 7 *March* 1991 *and in final form* 20 *August* 1991)

Abstract—A combined experimental and analytical study of reflux condensation phenomena in single vertical tubes with large l/D ratios was conducted. From the experimental observations made, phenomenological modelling was conducted by combining an extension of the classical Nusselt theory with a linearized stability analysis of the condensate film flow. A comparison between the model and the corresponding experimental data is presented and discussed. The satisfactory agreement between the model and the data indicates that this model could be used in nuclear reactor accident analysis to estimate heat removal capabilities of U-tube steam generators when, on the tube side, the assumed heat rejection mechanism is total reflux condensation.

1. INTRODUCTION

UNDER normal operating conditions the fuel rods in a CANDU-PHWR‡ or a PWR§ are well cooled by the coolant circulated by the primary pumps. This mode of fuel cooling may be disrupted or may deteriorate under various accident scenarios where loss of forced circulation occurs.

These accident scenarios define conditions where the U-tube steam generators act as important heat sinks. An illustration of this important possibility can be seen by considering a situation where heat (perhaps at decay levels) is generated in the reactor core and only a portion of it can be transported out through a small leak or break in the primary heat transport system. In this case, there may be some additional heat losses through the system piping components, but the steam generators become the major heat sinks [1].

Depending on the particulars of the accident scenario [2], such as the primary pumps rundown time, the location and size of the break and the details of the emergency core cooling system, different heat removal mechanisms may occur in the steam generator tubes. These include reflux condensation, single- and two-phase thermosyphoning. In general, heat removal capability in natural circulation is greater than in reflux condensation. Therefore, it is of interest to determine the mechanisms governing heat removal in reflux condensation.

The existing data base for reflux condensation is primarily from idealized component experiments [3–6] where the *vertical* reflux tube had a ratio $l/D < 140$. Russell [7] did experiments in an *inclined* long reflux tube with $l/D = 250$; however, no detailed measurements of the characteristics of the two-phase condensing flow were performed. In U-tube steam generators, the l/D ratio can be very large (>700). To estimate their heat removal capabilities and the liquid hold-up when reflux condensation is the heat removal mechanism on the tube side, detailed knowledge of reflux condensation phenomena in tubes with large l/D ratio is needed. This paper reports the results of a combined experimental and analytical study of reflux condensation phenomena in single vertical tubes with large l/D ratios. Experimental observations of reflux condensation for an imposed constant pressure drop across the reflux tube is given. The phenomenological modelling of the experimental observations is conducted and a comparison between the model and the corresponding experimental data is presented and discussed. Although local parameters were measured in this work, only global parameters are used in the above comparison and the analysis of the local measurements will be the subject of a future paper.

2. EXPERIMENTAL OBSERVATIONS

To simplify the system as much as possible, an experimental apparatus as shown schematically in Fig. 1 was used in the present work. It consists of a series of eight consecutive double pipe heat exchangers made of pyrex glass linked together by Teflon spacers to allow measurements of pressures and temperatures at the centre and near the wall inside the inner tube and the injection of water in each cooling jacket. The void fraction was measured using capacitance probes. The inner tube is connected at the bottom to a steam inlet plenum and at the top to an outlet plenum. Both

† To whom correspondence should be addressed. Present address: Point Lepreau N.G.S., Safety Analysis Section, P.O. Box 10, Lepreau, N.B., E0G 2H0, Canada.

‡ Canada Deuterium Uranium—Pressurized Heavy Water Reactor.

§ Pressurized Water Reactor.

NOMENCLATURE

B $= \sqrt{(1+2F)}$

c_{pl} specific heat capacity of the condensate [J kg^{-1} °C^{-1}]

$\bar{c}$ $= \bar{c}_r + i\bar{c}_i$ non-dimensional complex eigenvalue

C_i constants in the solution of the eigenvalue problem

D_1, D_2, E functions in equation (37) and defined in the Appendix

f_i interfacial friction factor

F $= P_1\bar{\delta}^5/3$

$F_{ht}^{(i)}$ functions in equation (37) and defined in the Appendix

$F_t(u_*, \bar{c}_i)$ function defined by equation (37)

g gravitational constant [m s^{-2}]

G $= 1 - S/2(1/Re_0)(dRe_\delta^2/d\bar{x})$

G_1, G_2 functions in equation (37) and defined in the Appendix

h_{fg} latent heat [J kg^{-1}]

i $= \sqrt{-1}$

j_k volumetric flux for phase k [m s^{-1}]; $k = l, g$

k_l thermal conductivity of the condensate [W m^{-1} °C^{-1}]

$\bar{k}$ $= 2\pi\delta_0/\lambda$ non-dimensional wavenumber

Ku $= c_{pl}\Delta T_g/h_{fg}$ Kutateladze number

K_k $= \rho_k^{1/2} j_k/[g\sigma(\rho_l - \rho_g)]^{1/2}$ Kutateladze variable; $k = l, g$

L_1, L_2 functions in equation (37) and defined in the Appendix

L_{sp} single-phase length [m]

$L_{2\phi}$ two-phase length [m]

$\dot{m}_{fl}$ flooding steam mass flow rate [kg s^{-1}]

$\dot{m}_i$ inlet steam mass flow rate [kg s^{-1}]

M_r $= \mu_g/\mu_l$

N_l function in equation (37) and defined in the Appendix

p pressure [N m^{-2}]

$\bar{p}$ $= p/\rho_l u_0^2$ non-dimensional pressure

p_{bp} bottom plenum pressure [k N m^{-2}]

p_{up} upper plenum pressure [k N m^{-2}]

Δp_{sp} pressure drop across the single-phase region [k N m^{-2}]

Pe $= PrRe_0$ Peclet number for the condensate film

Pr $= \mu_l/c_{pl}k_l$ Prandlt number for the condensate film

P_l $= f_i S Re_0$

P_s non-dimensional normal perturbation stress

$\dot{q}_0$ heat flux at the inner wall of the tube [W m^{-2}]

r radial coordinate [m]

R inner radius of the tube [m]

$\bar{R}$ $= R/\delta_0$ non-dimensional inner radius

Re_δ $= \Gamma/\mu_l$ film Reynolds number

Re_0 $= \rho_l u_0 \delta_0/\mu_l$ Reynolds number

S $= 4\rho_l/\rho_g(1/\bar{R}^2)$

$S(y)$ condensate film disturbance temperature amplitude [°C]

$\bar{S}(\bar{y})$ $= S(y)/\Delta T_g$ non-dimensional condensate film disturbance temperature amplitude

$T_{cw,i}$ cooling water inlet temperature [°C]

T_l condensate film temperature [°C]

$\bar{T}_l$ $= (T_l - T_{sat})/\Delta T_g$ non-dimensional condensate film temperature

T_{sat} saturation temperature corresponding to the bottom plenum pressure [°C]

T_p non-dimensional higher order polynomial in η

ΔT_q $= \dot{q}_0'' \delta_0/k_l$ reference temperature difference [°C]

T_s non-dimensional tangential perturbation stress

u_g axial steam velocity [m s^{-1}]

u_l axial condensate velocity [m s^{-1}]

$u_{g,cl}$ axial steam velocity at the tube centre line [m s^{-1}]

u_g^+ non-dimensional local axial steam velocity

u_* $= \sqrt{(f_{ic} u_{g,cl}^2/2)}$ friction velocity [m s^{-1}]

$\bar{u}_l$ $= u_l/u_0$ non-dimensional axial condensate velocity

u_{li} interfacial condensate film velocity [m s^{-1}]

$\bar{u}_{li}$ non-dimensional interfacial condensate film velocity [m s^{-1}]

u_0 $= g(\rho_l - \rho_g)\delta_0^2/2\mu_l$ interfacial condensate film velocity with no interfacial drag [m s^{-1}]

v_l transversal condensate film velocity [m s^{-1}]

$\bar{v}_l$ $= v_l/u_0$ non-dimensional transversal condensate film velocity

x axial coordinate [m]

$\bar{x}$ $= x/\delta_0$ non-dimensional axial coordinate

y transversal coordinate [m]

$\bar{y}$ $= y/\delta_0$ non-dimensional transversal coordinate.

Greek symbols

$\beta_1, \beta_2, \beta_3$ functions in equations (33) and (34), and defined in the Appendix

γ $= \rho_g/\rho_l$

Γ condensate mass flow rate per unit width [kg m^{-1} s^{-1}]

δ base flow film thickness [m]

$\bar{\delta}$ $= \delta/\delta_0$ non-dimensional base flow film thickness

δ_0 base flow film thickness at the tube entrance [m]

ζ thickness of the wavy film [m]

η $= \bar{y}/\bar{\delta}$ non-dimensional transversal coordinate

NOMENCLATURE (Contd.)

λ	wavelength [m]
μ_l	absolute viscosity of the condensate film [kg m^{-1} s^{-1}]
μ_g	absolute viscosity of the steam [kg m^{-1} s^{-1}]
ρ_l	condensate film density [kg m^{-3}]
ρ_g	steam density [kg m^{-3}]
σ	surface tension [N m^{-1}]
$\phi(y)$	disturbance stream function amplitude in the condensate film [m^2 s^{-1}]
$\bar{\phi}(\bar{y})$	$= \phi(y)/u_0\delta_0$ non-dimensional disturbance stream function amplitude in the condensate film.

Subscripts

g	steam phase
g, cl	steam phase at the centre line of the tube
ie	interface of condensate film and steam at the tube entrance
k	phase considered, $k = l, g$
li	interface of condensate film and steam
sp	single-phase liquid
up	upper plenum
2ϕ	two-phase
0	tube entrance.

Superscripts

(i)	imaginary part of function $F_t(u_*, \bar{c}_i)$
(r)	real part of function $F_t(u_*, \bar{c}_i)$
$\bar{}$	non-dimensional variable.

plenums were thermally insulated with glass wool. The experiments were conducted with three different tube sizes: 2.54, 1.91 and 1.27 cm o.d. (respectively 2.06, 1.59 and 0.95 cm i.d.). The total length of the tubes was 4.8 m, giving l/D ratios of respectively 233, 303 and 506. Further details can be found elsewhere [8].

Figure 2 illustrates in a schematic way the phenomena observed for an increasing imposed pressure drop corresponding to an increasing steam mass flow rate. Each situation shown represents the same inner tube of the present reflux condenser with the two-phase flow pattern corresponding to a different imposed constant pressure drop. To go from one flow pattern to another, the steam flow was adjusted until the desired flow pattern was seen.

Before flooding occurs, the phenomena observed were similar to what occurs in a short reflux condenser [3–6]. Flooding in a short reflux condenser causes the condensate to be ejected from the top; however, the phenomena observed in the present system were different: when the flooding point was reached, the condensate, instead of being ejected from the tube, was ejected from the average condensation (two-phase) region to accumulate in the form of a water column (single-phase region). In the case where a new constant pressure drop is imposed across the tube for a situation with a water column oscillating over the two-phase region, the system undergoes a small transient, in which the flooding point is reached, resulting in a new quasi-static situation with a water column of increased length oscillating over a two-phase region of unchanged average length. Each of the flow regimes shown in the last four tubes in Fig. 2 is an example of a quasi-static situation observed that could be held indefinitely, where the average lengths of the single-phase and the two-phase regions remain constant. For these later situations, the condensate level meter of the bottom plenum indicated that a significant amount of condensate was collected in the bottom plenum. In all the situations shown in Fig. 2, all the injected steam is condensed and its condensate flowed back counter-current to the upward steam flow. In the present study, this flow regime is called total reflux condensation and could be qualified as quasi-static.

The flow pattern observed in the two-phase region was intermittent churn-annular counter-current flow with entrainment in the form of droplet aggregates in the vapour core, pulsating upward towards the end of the two-phase region. These droplet aggregates were observed to originate from the formation of a standing wave near the tube inlet and the accumulation of condensate above it. The action of the vapour flow was then to tear off part of the accumulated condensate (including the condensate in the wave) forming the droplet aggregates. In vertical two-phase flow the slug flow pattern can be described as a succession of cap-shaped bubbles moving upward with the region between the bubbles being mostly filled by liquid. So, the liquid plays the role of the matrix in that flow pattern. In the present study, the flow pattern observed, in the vapour core alone, could be called an 'inverted-slug' flow where the matrix of flow pattern is the vapour phase and the role of the cap-shaped bubbles is played by the droplet aggregates.

The flooding criterion used in this study can be pictured as being the point where the steam flow rate is such that a water column starts to build up, resulting in a change in the bottom plenum pressure. Another definition of the flooding criterion can be stated as being the point where the steam flow rate is such that a standing wave, with respect to the condensate film interfacial velocity, appears near the tube inlet and a net transport of condensate occurs by means of droplet aggregates pulsating upward. The two criteria are considered to be equivalent because it is the net transport of condensate upward that gives rise to the presence of a water column, which in turn is the cause of an increase in the bottom plenum pressure. In the present study the first definition was used as the flood-

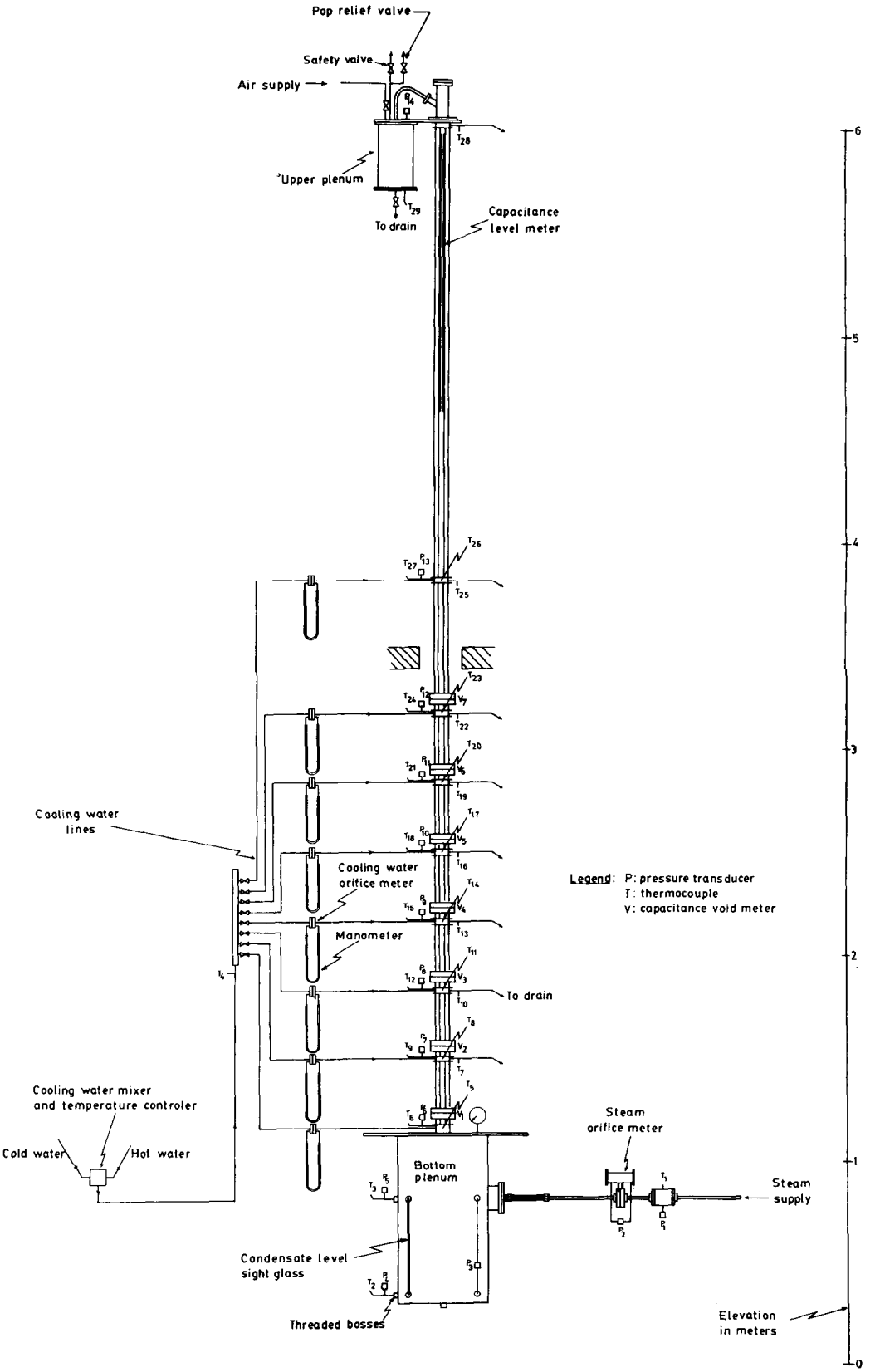

FIG. 1. Schematic of the reflux condenser.

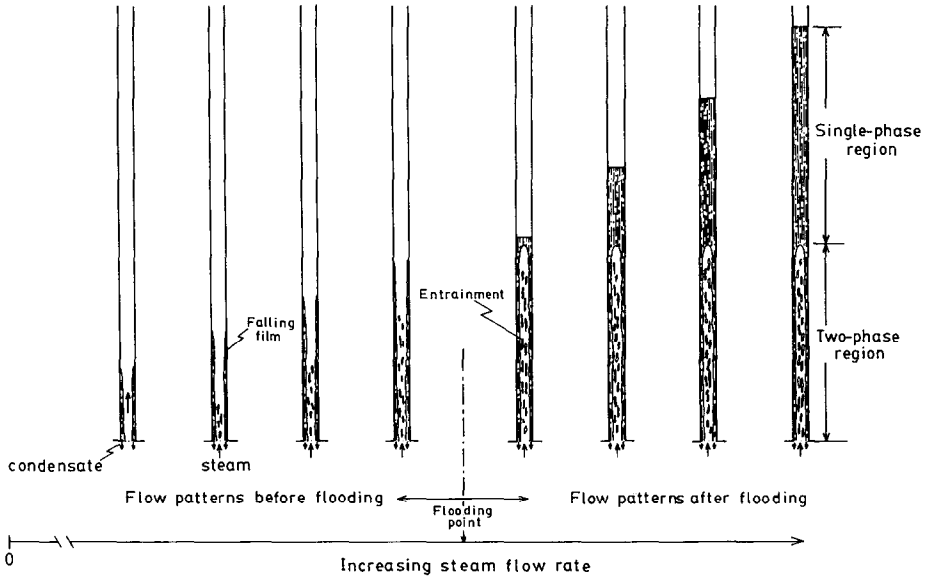

FIG. 2. Flow patterns observed for an imposed pressure drop across the tube.

ing criterion in all the experimental work, because it is reproducible and easily traceable. The other formulation is simply the one used by Cetinbudaklar and Jameson [9] and it is used, as presented later, in the linearized stability analysis of the condensate film flow.

3. MATHEMATICAL MODELLING

3.1. *An extended Nusselt theory*

The exact mathematical modelling of reflux condensation is quite formidable because of the countercurrent nature of the flow and the complex pattern of the waves travelling on the steam–water interface. Extensive idealizations are required to simplify the governing equations if any solution, either analytical or numerical, is to be obtained. In Fig. 3, we show the idealization of the configuration of the flow pattern used in the present base flow model. The assumptions made are: (i) the flow pattern is steady-state countercurrent annular flow with no entrainment from the film in the vapour core and with a smooth interface; (ii) the flow of condensate in the film is laminar; (iii) the film thickness of the condensate is negligibly small when compared to the tube inner radius; (iv) the axial velocity profile in the vapour core is nearly uniform and much greater than the interfacial condensate film velocity; (v) the pressure is the same in each phase and is only a function of the axial position 'x'; (vi) the heat flux at the inner wall of the tube is constant; (vii) the thermal-hydraulic properties of both phases are constant and evaluated at saturation where the saturation pressure is taken to be the bottom plenum pressure; (viii) the condensation shear stresses at the steam–water interface have small influence on the characteristics of the base flow.

The methodology used is similar to the one in the classical Nusselt theory [10] and is as follows: (i) obtain the radial and axial velocity profiles in the condensate film in terms of the film thickness by solving the liquid phase momentum with the aid of the vapour phase momentum equation and the continuity equation of each phase; (ii) obtain the condensate film temperature profile, again in terms of the film thickness, by using the velocity profiles in solving the energy equation; (iii) then, obtain the differential equation for the film thickness by substituting the

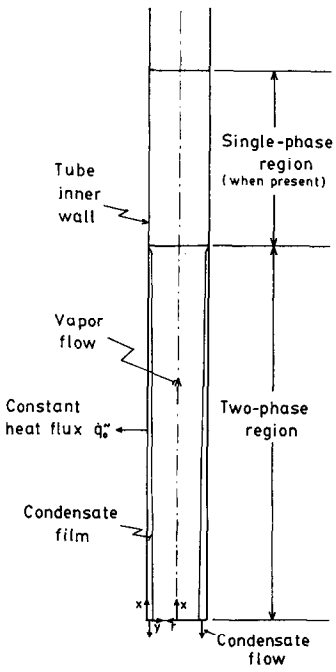

FIG. 3. Flow pattern idealization of total reflux condensation.

temperature profile in the equation resulting from the combination of the heat and mass interfacial jump conditions.

The geometry of the system being cylindrical, the local instantaneous conservation equations can be written as follows:

mass conservation

$$\frac{\partial}{\partial x}(\rho_l r u_l)+\frac{\partial}{\partial r}(\rho_l r v_l)=0 \tag{1}$$

$$\frac{\partial}{\partial x}(\rho_g r u_g)+\frac{\partial}{\partial r}(\rho_g r v_g)=0 \tag{2}$$

momentum conservation

$$\frac{\partial}{\partial x}(\rho_l u_l^2 r)+\frac{\partial}{\partial r}(\rho_l u_l v_l r) = -r\frac{\partial p}{\partial x}+\mu_l\frac{\partial}{\partial r}\left(r\frac{\partial u_l}{\partial r}\right)-g(\rho_l-\rho_g)r \tag{3}$$

$$\frac{\partial}{\partial x}(\rho_g u_g^2 r)+\frac{\partial}{\partial r}(\rho_g u_g v_g r) = -r\frac{\partial p}{\partial x}+\mu_g\frac{\partial}{\partial r}\left(r\frac{\partial u_g}{\partial r}\right)-g(\rho_g)r \tag{4}$$

energy conservation

$$\frac{\partial}{\partial x}(r\rho_l c_{pl} u_l T_l)+\frac{\partial}{\partial r}(r\rho_l c_{pl} v_l T_l)=k_l\frac{\partial}{\partial r}\left(r\frac{\partial T_l}{\partial r}\right). \tag{5}$$

Before deriving the velocity profile in the condensate film, we first state, based on the first assumption, that mass conservation is satisfied at each cross-section of the two-phase region. Then, we can write:

$$-\int_{R-\delta(x)}^{R}\rho_l u_l r\,dr = R\Gamma = \int_0^{R-\delta(x)}\rho_g u_g r\,dr. \tag{6}$$

The integration of condensate and vapour momentum equations respectively from $r=R-\delta(x)$ to $r=R$ and from $r=0$ to $r=R-\delta(x)$, combined with the integration of their respective mass conservation equations and the use of the Leibnitz formula [11], gives an expression for the pressure gradient. This is further simplified using the non-slip conditions at the steam–water interface. The resulting expression for the pressure gradient is then introduced in the condensate momentum equation to obtain:

$$\rho_l u_l\frac{\partial u_l}{\partial x}+\rho_l v_l\frac{\partial v_l}{\partial r}=\mu_l\frac{1}{r}\frac{\partial}{\partial r}\left(r\frac{\partial u_l}{\partial r}\right)-g(\rho_l-\rho_g) -2\frac{\mu_l}{R}\left(\frac{\partial u_l}{\partial r}\right)_R-\frac{(2R\delta-\delta^2)}{R^2}g(\rho_l-\rho_g)+\frac{2}{R^2}\frac{d}{dx} \times\int_0^{R-\delta(x)}\rho_g u_g^2 r\,dr+\frac{2}{R^2}\frac{d}{dx}\int_{R-\delta(x)}^{R}\rho_l u_l^2 r\,dr. \tag{7}$$

In the present study, the condensation process occurs in the presence of a body force (gravity) and forced convection of the steam and the condensate at a Prandtl number greater than or equal to one. For a flow of that type, one can neglect the inertia terms in the condensate momentum equation [12], i.e. in equation (7) the left-hand side and the last term on the right-hand side can be dropped. Using equation (6) and the fourth assumption, one can write the following approximation:

$$\frac{2}{R^2}\frac{d}{dx}\int_0^{R-\delta(x)}\rho_g u_g^2 r\,dr=\frac{4}{\rho_g R^2}\frac{d}{dx}\Gamma^2. \tag{8}$$

Introducing the change in coordinate $y=R-r$, where 'y' is the transverse coordinate as shown in Fig. 3, and simplifying equation (7), one can write the equation of motion for the condensate film as follows:

$$\mu_l\frac{\partial^2 u_l}{\partial y^2}-g(\rho_l-\rho_g)+\frac{4}{\rho_g R^2}\frac{d}{dx}\Gamma^2=0 \tag{9}$$

with the following boundary conditions:

B.C.1 at $y=0;\quad u_l=0$

B.C.2 at $y=\delta;$

$$\mu_l\frac{\partial u_l}{\partial x}=\frac{f_i}{2}\rho_g(u_g-u_{li})|u_g-u_{li}|.$$

The integration of equation (9) with the application of the boundary conditions gives in non-dimensional form:

$$\bar{u}_l=(\bar{y}^2-2\bar{\delta}\bar{y})-\frac{S}{2}\frac{1}{Re_0}\frac{d^2Re_\delta^2}{dx^2}(\bar{y}^2-\bar{\delta}\bar{y}) +\frac{f_i}{2}\frac{S}{Re_0}Re_\delta^2\,\bar{y} \tag{10}$$

and from the mass conservation equation, the transverse velocity profile is:

$$\bar{v}_l=G\frac{d\bar{\delta}}{d\bar{x}}\bar{y}^2+\frac{S}{2}\frac{1}{Re_0}\frac{d^2Re_\delta^2}{d\bar{x}^2}\left(\frac{\bar{y}^3}{3}-\bar{\delta}\bar{y}\right) +\frac{S}{2}\frac{1}{Re_0}\frac{df_i}{d\bar{x}}Re_\delta^2\frac{\bar{y}^2}{2}+\frac{f_i}{2}\frac{S}{Re_0}\frac{dRe_\delta^2}{d\bar{x}}\frac{\bar{y}^2}{2}. \tag{11}$$

The energy conservation equation for the condensate film in non-dimensional form can be written as:

$$\bar{u}_l\frac{\partial\bar{T}_l}{\partial\bar{x}}+\bar{v}_l\frac{\partial\bar{T}_l}{\partial\bar{y}}=\frac{1}{Pe}\frac{\partial^2\bar{T}_l}{\partial\bar{y}^2} \tag{12}$$

with the following boundary conditions:

B.C.1 at $\bar{y}=0;\quad \frac{\partial\bar{T}_l}{\partial\bar{y}}=1$

B.C.2 at $\bar{y}=\bar{\delta};\quad \bar{T}_l=0.$

Rohsenow [13] modified Nusselt theory by relaxing one of the basic assumptions [10]: the heat transfer is by conduction and convection. Although Rohsenow analysis differs from the present study, one could assume in the present derivation a temperature profile having a form similar to his:

$$\bar{T}_l = \eta + \bar{T}_p \tag{13}$$

where $\bar{T}_p = \bar{T}_p(\eta)$ is a higher order polynomial. Introducing equations (10), (11) and (13) in equation (12) and keeping first order terms only, we obtain:

$$\frac{d^2\bar{T}_p}{d\eta^2} = \left\{ -G\eta^3 + 3G\eta^2 - \frac{f_i S}{2Re_0}\frac{Re_\delta^2}{\bar{\delta}}\eta^2 + \frac{dG}{d\bar{\delta}}\bar{\delta}\left(\frac{\eta^3}{3} - \eta^2\right) + \frac{f_i S}{2Re_0}\frac{dRe_\delta^2}{d\bar{\delta}}\frac{\eta^2}{2}\right\} Pe\bar{\delta}^3\frac{d\bar{\delta}^3}{d\bar{x}} \tag{14}$$

with the following boundary conditions:

B.C.1 at $\eta = 0$; $\dfrac{d\bar{T}_p}{d\eta} = \bar{\delta} - 1$

B.C.2 at $\eta = 1$; $\bar{T}_p = 1$.

Integration of equation (14) with the application of its boundary conditions and simplification by an order of magnitude analysis of the resulting expression give:

$$\bar{T}_l = \bar{\delta}(\eta - 1) + \left\{ -\frac{G}{20}(\eta^5 - 1) + \frac{G}{4}(\eta^4 - 1) + \frac{f_i}{24} S \frac{Re_\delta}{Re_0}\frac{dRe_\delta}{d\bar{\delta}}(\eta^4 - 1) - \frac{f_i}{24}\frac{S}{\bar{\delta}}\frac{Re_\delta^2}{Re_0}(\eta^4 - 1)\right\} Pe\bar{\delta}^3\frac{d\bar{\delta}^3}{d\bar{x}}. \tag{15}$$

The mass and energy jump conditions can be written as [14]:

mass

$$\rho_l\left\{v_l - \left[\frac{\partial\zeta}{\partial t} + u_l\frac{\partial\zeta}{\partial x}\right](1-\gamma)\right\} = \rho_g v_g \tag{16}$$

energy

$$\rho_g v_g h_{fg} = -k_l\frac{\partial T_l}{\partial y}. \tag{17}$$

The right-hand side of equation (16) is the condensation mass transfer, and conservation of mass at each cross-section of the two-phase region results in:

$$\frac{d\Gamma}{dx} = \rho_g v_g. \tag{18}$$

Introducing equation (18) in equation (17) we obtain in non-dimensional form:

$$\frac{dRe_\delta}{d\bar{x}} = -\frac{Ku}{Pr}\left(\frac{\partial\bar{T}_l}{\partial\bar{y}}\right)_{\bar{y}=\bar{\delta}}. \tag{19}$$

By definition we have:

$$Re_\delta = \frac{\Gamma}{\mu_l} = -\int_0^\delta \rho_l\frac{u_l}{\mu_l}dy. \tag{20}$$

Introducing equation (10) in equation (20) we obtain:

$$Re_\delta = \frac{4}{3}\frac{Re_0\bar{\delta}^3}{1+\sqrt{(1+2F)}}. \tag{21}$$

Introducing equations (15) and (21) in equation (19) the following differential equation for the dimensionless film thickness is obtained:

$$Re_0\frac{Pr}{3Ku}\frac{d\bar{\delta}^3}{d\bar{x}} = -\left[\frac{4}{1+B_l} - \frac{20}{3}\frac{F}{B_l(1+B_l)^2} + Ku \times \left\{\frac{3}{4} + \frac{8}{3}\frac{F}{(1+B_l)^2}\left[\frac{11}{3} - \frac{40}{9}\frac{F}{B_l(1+B_l)}\right]\right\}\right]^{-1}. \tag{22}$$

From the momentum equation and the no-slip conditions the pressure gradient can be written as:

$$\frac{\partial\bar{p}}{\partial\bar{x}} = -\left[\frac{4}{\gamma}\frac{1}{Re_0^2}\frac{1}{\bar{R}^2}\frac{dRe_\delta^2}{d\bar{x}} + \frac{f_i}{\bar{R}}\frac{S}{Re_0^2}Re_\delta^2\right]. \tag{23}$$

The interfacial friction factor is calculated from the Baharathan–Wallis correlation [15].

In summary, equations (6), (15), (21), (22) and (23) are the governing equations of the present model of film-wise condensation. Similar results were reported recently [16] for a short reflux condenser ($l/D = 14.6$) with a different inner wall boundary condition than in the present study: the inner wall was assumed to be at constant temperature. Another difference is the choice of the characteristic length and the condensate velocity used in putting the equations in non-dimensional form, which is common to both the extended Nusselt theory and, as will be shown below, to the stability analysis. The choice of the constant inner wall heat flux as boundary condition is based on the experimental evidence that the cooling side heat transfer resistance is much larger than the one on the condensing side. Experimental data from steam condensation on a horizontal cylinder with a high cooling side heat transfer resistance are shown to be in better agreement with a theory based on the constant wall heat flux boundary condition [17], giving support to the choice of boundary condition just made. This completes the presentation of the present extended Nusselt theory.

3.2. *A linearized stability analysis of film-wise condensation*

In this section a linearized stability analysis of film-wise condensation is exposed and its purpose is to compute the steam flow rate that leads to flooding for a prescribed base flow. It differs from previous studies by the nature of the perturbations considered, their consequences and the inclusion of tube diameter, surface tension and viscosity effects. In the present system the condensate film is perturbed by counter-current condensing steam flow. Then, the perturbations considered are those related to the hydrodynamics of the two-phase flow and the condensation mass transfer. Moreover, it is hypothesized that they cause the formation of standing waves which in turn, as mentioned above, lead to flooding. A linearized stability analysis can give the interesting result of being able to identify the relative strength of each component of the net force acting on the interface. That knowledge could

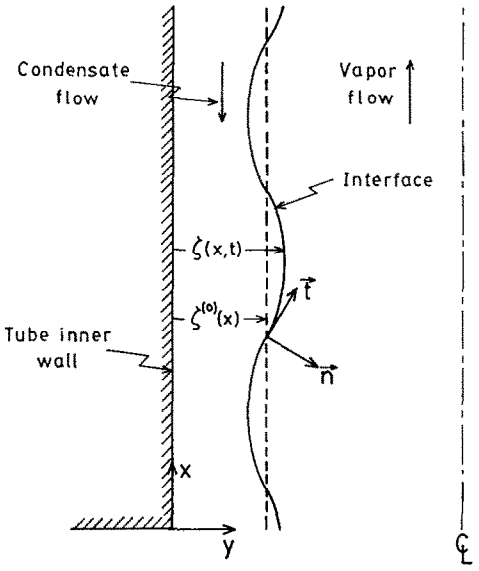

FIG. 4. Flow situation idealization near the tube inlet.

give justifications of the assumptions that would be made in the derivation of simpler models.

In Fig. 4 the idealized flow situation near the tube entrance is shown. The assumptions made in the present stability study are: (i) flooding occurs at the tube inlet; (ii) the velocity profile in the steam core is no longer assumed to be flat, instead the universal velocity profile [18] is assumed to be valid; (iii) the local approximation method [19] is valid for the present case of film-wise condensation; (iv) the amplitude of the wave is assumed to be infinitesimal and its wavelength is considered to be long with respect to the base flow film thickness. In the study of the stability of flow, the problem can be reduced to an eigenvalue problem formulated in terms of the governing equations for the disturbance amplitude functions and their boundary and interfacial disturbance jump conditions. The detailed derivations of the two governing equations for the disturbance amplitude functions and the boundary conditions have been reported previously [19–21] and will be omitted. On the other hand, the appropriate expressions of the interfacial disturbance jump conditions for the present problem have not been exposed in the open literature yet and their detailed derivations can be found in ref. [8]. The statement of the eigenvalue problem for the present study is as follows:

(i) the Orr–Sommerfeld equation

$$\frac{\mathrm{d}^4\bar{\phi}}{\mathrm{d}\bar{y}^4}-2\bar{k}^2\frac{\mathrm{d}^2\bar{\phi}}{\mathrm{d}\bar{y}^2}+\bar{k}^4\bar{\phi}(\bar{y})=i\bar{k}Re_0\times\left[(\bar{u}_1^{(0)}-\bar{c}^{(0)})\frac{\mathrm{d}^2\bar{\phi}}{\mathrm{d}\bar{y}^2}-\bar{k}^2\bar{\phi}(\bar{y})-\frac{\partial^2\bar{u}_1^{(0)}}{\partial\bar{y}^2}\bar{\phi}(\bar{y})\right] \tag{24}$$

(ii) the perturbed energy equation

$$\frac{\mathrm{d}^2\bar{S}}{\mathrm{d}\bar{y}^2}-\bar{k}^2\bar{S}(\bar{y})=i\bar{k}Pe\left[(\bar{u}_1^{(0)}-\bar{c}^{(0)})\bar{S}(\bar{y})-\frac{\partial\bar{T}_1^{(0)}}{\partial\bar{y}}\bar{\phi}(\bar{y})\right] \tag{25}$$

(iii) the boundary conditions

B.C.1 at $\bar{y}=0;\quad \bar{\phi}(0)=0$ (26)

B.C.2 at $\bar{y}=0;\quad \dfrac{\mathrm{d}\bar{\phi}(0)}{\mathrm{d}\bar{y}}=0$ (27)

B.C.3 at $\bar{y}=0;\quad \dfrac{\mathrm{d}\bar{S}(0)}{\mathrm{d}\bar{y}}=0$ (28)

B.C.4 at

$$\bar{y}=\delta;\quad (\bar{u}_1^{(0)}-\bar{c}^{(0)})\bar{S}(\bar{y})-\frac{i}{\bar{k}}\frac{\partial\bar{T}_1^{(0)}}{\partial\bar{y}}\frac{Ku}{Pe}\frac{\mathrm{d}\bar{S}}{\mathrm{d}\bar{y}}-\frac{\partial\bar{T}_1^{(0)}}{\partial\bar{y}}\bar{\phi}(\bar{y})=0 \tag{29}$$

(iv) momentum jump condition (normal projection)

$$\begin{aligned}&i(\bar{u}_1^{(0)}-\bar{c}^{(0)})\left[\frac{\mathrm{d}^3\bar{\phi}}{\mathrm{d}\bar{y}^3}-3\bar{k}^2\frac{\mathrm{d}\bar{\phi}}{\mathrm{d}\bar{y}}\right]-\bar{k}(\bar{u}_1^{(0)}-\bar{c}^{(0)})\\&\times Re_0\left[\frac{\partial\bar{u}_1^{(0)}}{\partial\bar{y}}\bar{\phi}(\bar{y})-(\bar{u}_1^{(0)}-\bar{c}^{(0)})\frac{\mathrm{d}\bar{\phi}}{\mathrm{d}\bar{y}}\right]\\&-\left[\bar{k}^2WeRe_0-P_s+2\bar{k}^2\frac{M_r}{\gamma}\frac{Ku}{Pe}\frac{\partial\bar{T}_1^{(0)}}{\partial\bar{y}}\right]\\&\times\left(\bar{k}\bar{\phi}(\bar{y})+i\frac{Ku}{Pe}\frac{\mathrm{d}\bar{S}}{\mathrm{d}\bar{y}}\right)+\bar{k}(\bar{u}_1^{(0)}-\bar{c}^{(0)})\\&\times\frac{2(1-\gamma)}{\gamma Re_0}\frac{Ku^2}{Pe^2}\frac{\partial\bar{T}_1^{(0)}}{\partial\bar{y}}\frac{\mathrm{d}\bar{S}}{\mathrm{d}\bar{y}}=0\end{aligned} \tag{30}$$

(v) momentum jump condition (tangential projection)

$$\left(T_s-\frac{\partial^2\bar{u}_1^{(0)}}{\partial\bar{y}^2}\right)\bar{\phi}(\bar{y})+\left[\frac{\mathrm{d}^2\bar{\phi}}{\mathrm{d}\bar{y}^2}-\bar{k}^2\frac{\mathrm{d}\bar{\phi}}{\mathrm{d}\bar{y}}\right](\bar{u}_1^{(0)}-\bar{c}^{(0)})-\frac{i}{\bar{k}}\frac{Ku}{Pe}\left(T_s-\frac{\partial^2\bar{u}_1^{(0)}}{\partial\bar{y}^2}\right)\frac{\mathrm{d}\bar{S}}{\mathrm{d}\bar{y}}=0. \tag{31}$$

The above eigenvalue problem needs expressions for P_s and T_s. Their full expressions have already been presented [9] and they will be omitted here. For a given base flow, the above eigenvalue problem contains five parameters: Re_0, $\bar{k}$, u_*, $\bar{c}_r$ and $\bar{c}_i$. Of these the Reynolds number is specified by the given base flow and the non-dimensional wavenumber is considered as given. As hypothesized before, at the flooding point standing waves appear on the interface near the tube inlet. This statement indicates that the wave celerity is equal to the interfacial condensate film velocity at the tube inlet, and we have:

$$\bar{c}_r=\bar{u}_{li}\quad\text{at}\quad\bar{x}=0. \tag{32}$$

In total reflux condensation, u_{li} depends on the inlet

steam flow rate which in turn is related to u_*. Then, at the flooding point there is a relation between the friction velocity and the wave celerity, i.e. knowing one will give the other. The above eigenvalue problem will furnish two eigenfunctions $\bar{\phi}(\bar{y})$ and $\bar{S}(\bar{y})$ and one complex eigenvalue $\bar{c} = \bar{c}_r + i\bar{c}_i$ for each pair of values $\bar{k}$ and Re_0. However, taking the same approach as Cetinbudaklar and Jameson [9], it is the friction velocity and the amplification factor $\bar{k}\bar{c}_i$ that are computed first and by the above relationships, the complex eigenvalue $\bar{c}$ is obtained.

In the present study, the method of Anshus and Goren [22] has been used for solving the eigenvalue problem. Following Spindler [19], the solution of the system at $\bar{x} = 0$ can be written as:

$$\bar{\phi}(\bar{y}) = C_1 \sin\beta_1\bar{y} + C_2\cos\beta_1\bar{y} + C_3\sin\beta_2\bar{y} + C_4\cos\beta_2\bar{y} \quad (33)$$

$$\bar{S}(\bar{y}) = C_5\sin\beta_1\bar{y} + C_6\cos\beta_1\bar{y} + C_7\sin\beta_2\bar{y} + C_8\cos\beta_2\bar{y} + C_9\sin\beta_3\bar{y} + C_{10}\cos\beta_3\bar{y}. \quad (34)$$

The introduction of equations (33) and (34) in the system of differential equations and application of the first two boundary conditions result in the following solution:

$$\bar{\phi}(\bar{y}) = C_1\left[\sin\beta_1\bar{y} - \frac{\beta_1}{\beta_2}\sin\beta_2\bar{y}\right] - C_2(\cos\beta_1\bar{y} - \cos\beta_2\bar{y}) \quad (35)$$

$$\bar{S}(\bar{y}) = C_1\left[\frac{L_1}{N_1}\sin\beta_1\bar{y} - \left(\frac{L_1}{N_2} - \frac{\beta_1}{\beta_2}\right)\sin\beta_2\bar{y}\right] + C_2\left[\frac{L_1}{N_1}\cos\beta_1\bar{y} - \frac{L_1}{N_2}\cos\beta_2\bar{y}\right] + C_9\sin\beta_3\bar{y} + C_{10}\cos\beta_3\bar{y}. \quad (36)$$

The introduction of equations (35) and (36) in equations (28)–(31) results in a homogeneous system of linear equations for the constants C_1, C_2, C_9 and C_{10}. At the tube inlet $\bar{x} = 0$, and at the interface we have $\bar{y} = \bar{\delta} = 1$. A non-trivial solution for these constants exists if the determinant of the coefficients is equal to zero. The determinant is shown in Fig. 5, where the definitions of the variables, not already defined explicitly in the Nomenclature, are given in the Appendix. After straightforward algebraic manipulations the determinant reduces to the following algebraic equation:

$$\begin{aligned} F_t(u_*, \bar{c}_i) &= \beta_1\beta_2(G_1D_1 + G_2D_2) \\ &\quad - \beta_1\beta_2(G_1D_2 + G_2D_1)\cos\beta_1\cos\beta_2 \\ &\quad - [G_1D_2\beta_2^2 + G_2D_1\beta_1^2]\sin\beta_1\sin\beta_2 \\ &\quad - \beta_1 E(\beta_2^2 - \beta_1^2)\sin\beta_2\cos\beta_1 \\ &\quad + \beta_2 E(\beta_2^2 - \beta_1^2)\sin\beta_1\cos\beta_2 + Ku\frac{\partial\bar{T}_1}{\partial\bar{y}} \\ &\quad \times\left[-F_{ht}^{(1)} + \frac{iF_{ht}^{(2)}}{\bar{k}Pe} - 2i\bar{k}^2\frac{Ku}{Pr}\frac{\partial\bar{T}_1}{\partial\bar{y}}\right. \\ &\quad \left.\times(F_{ht}^{(3)} + F_{ht}^{(4)}) - EF_{ht}^{(5)} + F_{ht}^{(6)} - F_{ht}^{(7)} + F_{ht}^{(8)}\right]. \end{aligned} \quad (37)$$

By its complex mathematical nature, equation (37) reduces to a set of non-linear algebraic equations as follows:

$$F_t^{(r)}(u_*, \bar{c}_i) = 0 \quad (38)$$

$$F_t^{(i)}(u_*, \bar{c}_i) = 0 \quad (39)$$

where $F_t^{(r)}$ and $F_t^{(i)}$ are the real and imaginary parts of F_t respectively. In the present study the method of Powell [23] has been used to solve the set of equations (38) and (39). The nature of the elements of equation (37) can be identified easily. All the terms in the square bracket multiplied by the Kutateladze number and the temperature gradient form an element related to heat transfer and all the remaining terms form an element related to the hydrodynamics of the two-phase flow.

3.3. *Simulation of total reflux condensation*

In the development of the model the following steps have been covered: (i) from visual observations two forms considered to be equivalent to the flooding criterion used in the present study have been defined; (ii) an extended Nusselt theory has been derived; (iii) a linearized stability analysis of the condensate film

$$\begin{vmatrix} L_1\beta_1\left(\frac{1}{N_1} - \frac{1}{N_2}\right) & 0 & \beta_3 & 0 \\ \beta_1\dot{c}\left(i(b_{10} - 3\bar{k}^2b_{11}) + \bar{k}Re_0\dot{c}b_{11} + a_6L_1b_{13}\right) - \left(a_4 + \bar{k}\dot{c}Re_0\frac{\partial\bar{u}_1^{(0)}}{\partial\bar{y}}\right)b_{12} + a_5L_1\beta_1b_{11} & \beta_1\dot{c}\left(i(b_{20} - 3\bar{k}^2b_{21}) + \bar{k}Re_0\dot{c}b_{21} + a_6L_1b_{22}\right) - \left(a_4 + \bar{k}\dot{c}Re_0\frac{\partial\bar{u}_1^{(0)}}{\partial\bar{y}}\right)b_{12} + a_5L_1\beta_1b_{22} & (a_5 + \dot{c}a_6)\beta_3\cos\beta_3 & -(a_5 + \dot{c}a_6)\beta_3\sin\beta_3 \\ \left(T_* - \frac{\partial^2\bar{u}_1^{(0)}}{\partial^2\bar{y}}\right)(b_{12} + a_1L_1\beta_1b_{13}) + (\beta_1c_{10} + \bar{k}^2b_{12})\dot{c} & \left(T_* - \frac{\partial^2\bar{u}_1^{(0)}}{\partial^2\bar{y}}\right)(b_{11} + a_7L_1\beta_1b_{22}) + (\beta_1c_{20} + \bar{k}^2b_{11})\dot{c} & a_7\left(T_* - \frac{\partial^2\bar{u}_1^{(0)}}{\partial^2\bar{y}}\right)\beta_3\cos\beta_3 & -a_7\left(T_* - \frac{\partial^2\bar{u}_1^{(0)}}{\partial^2\bar{y}}\right)\beta_3\sin\beta_3 \\ \dot{c}L_1d_{10} - a_1L_1\beta_1b_{13} - a_2b_{12} & \dot{c}L_1b_{13} - a_1L_1\beta_1b_{22} - a_2b_{11} & \dot{c}\sin\beta_3 - a_1\beta_3\cos\beta_3 & \dot{c}\cos\beta_3 + a_1\beta_3\sin\beta_3 \end{vmatrix} = 0$$

FIG. 5. Determinant of the system of homogeneous linear equations.

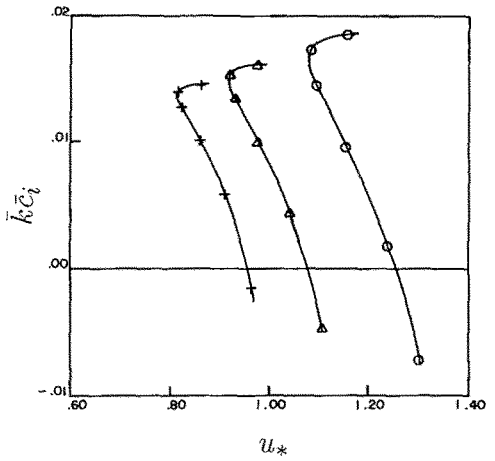

FIG. 6. Variations of the dimensionless amplification factor as a function of the interfacial friction velocity. (○) $Re_0 = 51.81$; (△) $Re_0 = 103.74$; (+) $Re_0 = 202.50$.

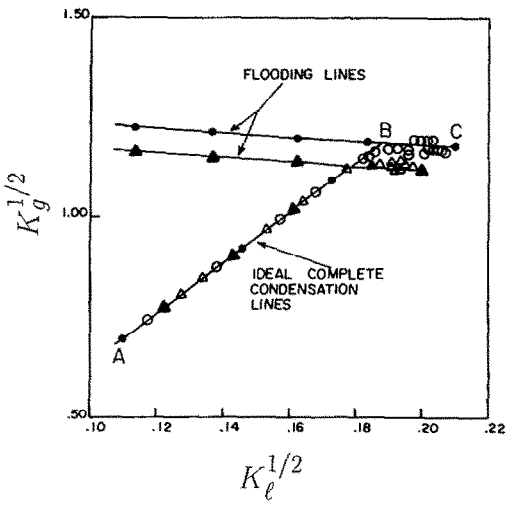

FIG. 7. Reflux condensation data in the $K_g^{1/2}$–$K_l^{1/2}$ plane for a 2.54 cm o.d. tube. (○) $T_{cw,i} = 10°C$; (△) $T_{cw,i} = 45°C$; (—●—) theory with $T_{cw,i} = 10°C$ and $f_{ie} = 0.0185$; (—▲—) theory with $T_{cw,i} = 45°C$ and $f_{ie} = 0.0227$.

has been carried out; (iv) the flooding criterion has been used to evaluate the wave celerity at the flooding point (see equation (32)); (v) the use of the critical layer concept reported in the literature on wave generation has been given in the form of constitutive equations for the perturbing stresses P_s and T_s.

For a given base flow condition, the only free parameter in equation (37) is the wavenumber and for each value of the wavenumber there corresponds one pair of roots of that equation. The question is now to determine the critical wavenumber (wavelength) that will correspond to a pair of roots that will be related to unstable flow conditions. The two concepts of maximum mechanical energy transfer and film instability can now be utilized to set up a simple criterion for the determination of that critical wavenumber. Figure 6 shows a variation of the non-dimensional amplification factor $\bar{k}\bar{c}_i$ as a function of the friction velocity u_* for a steam–water system at atmospheric pressure in a 2.54 cm o.d. tube with $f_{ie} = 0.0185$. Each curve corresponds to the solution of equation (37) for a range of wavenumbers with a given base flow condition indicated by the value of the Reynolds number. It can be seen that in the unstable region, where $\bar{k}\bar{c}_i > 0$, each curve goes through a minimum value of u_*. It is the pair of roots corresponding to that minimum u_* that is of greatest interest since it defines that value of u_* below which all individual oscillations decay, whereas above that value at least some are amplified. In other words, it corresponds to flow conditions when the transfer of mechanical energy is at its maximum and it is all absorbed by viscous dissipation in the condensate film, ensuring its stability. This smallest friction velocity is the limit of stability with respect to the type of flow under consideration. Then, the steam flow rate at the flooding point is computed as follows. First, the steam velocity at the centreline is computed from the definition of the friction velocity. Second, it is multiplied by the ratio of the average velocity to the centreline velocity computed with the 'universal velocity profile' to obtain the average velocity. Third, the average velocity is multiplied by the steam density and the actual cross-sectional area of the steam flow. The characteristics of a base flow are obtained by solving the governing equations of the present model arising from the extended Nusselt theory by applying global mass and energy balances. The simulation of the sequence of quasi-state situations shown in Fig. 2 is based on (i) the flooding criterion presented earlier, (ii) an extended Nusselt theory, (iii) a linearized stability analysis with the application of three concepts: critical layer, maximum mechanical energy transfer and film instability, and (iv) the postulate that after flooding is reached, the reflux condenser still operates at the flooding point, on a time average basis, for each new boundary condition defined by the new imposed pressure drop across the tube. It should be noted here the use of the same characteristic length 'δ_0' and the velocity 'u_0' in the present extended Nusselt theory and linearized stability analysis is to obtain a unified model of total reflux condensation. The results of the simulation are presented along with the experimental data in the following section, where a comparison is made.

4. COMPARISON OF NUMERICAL RESULTS WITH EXPERIMENTAL DATA

4.1. *Flooding*

One of the main features of total reflux condensation is the impossibility of independently varying the phase flow rates and temperatures as in the case of air–water or air–steam/water flooding experiments. The rates of condensation obtained for the three tubes have been plotted in the $K_g^{1/2}$–$K_l^{1/2}$ plane in Figs. 7–9 with the cooling water inlet temperature and the entrance interfacial friction factor ($T_{cw,i}$ and f_{ie} respec-

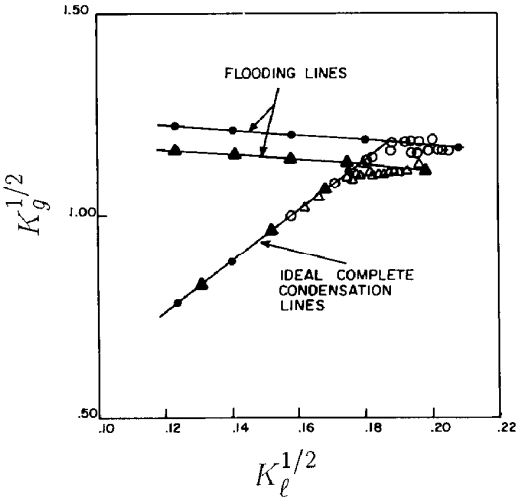

FIG. 8. Reflux condensation data in the $K_g^{1/2}$–$K_l^{1/2}$ plane for a 1.91 cm o.d. tube. (○) $T_{cw,i} = 14°C$; (△) $T_{cw,i} = 45°C$; (—●—) theory with $T_{cw,i} = 14°C$ and $f_{ie} = 0.0185$; (—▲—) theory with $T_{cw,i} = 45°C$ and $f_{ie} = 0.0227$.

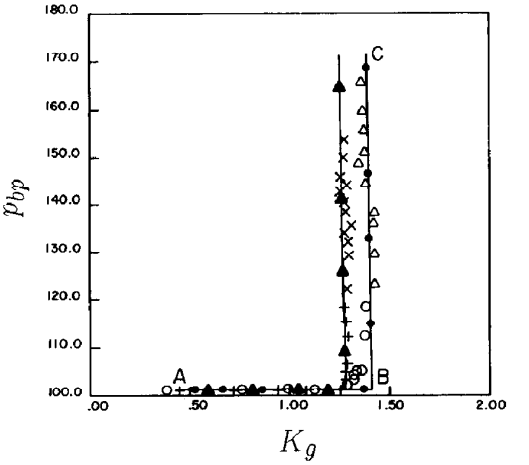

FIG. 10. Variations of the bottom plenum pressure as a function of steam flow rate for a 2.54 cm o.d. tube. (○) Upper plenum opened to atmosphere with $T_{cw,i} = 10°C$; (△) upper plenum pressurized with $T_{cw,i} = 10°C$; (+) opened to atmosphere with $T_{cw,i} = 45°C$; (×) upper plenum pressurized with $T_{cw,i} = 45°C$; (—●—) theory with $T_{cw,i} = 10°C$ and $f_{ie} = 0.0185$; (—▲—) theory with $T_{cw,i} = 45°C$ and $f_{ie} = 0.0227$.

tively in the figures) as the main parameters. It can be seen that in total reflux condensation, the steam and condensate flow rates on the flooding curves are, in terms of the Kutateladze variables, in the high and low range respectively when compared to the ranges of values these variables can have in an adiabatic system ($K_l^{1/2}$ and $K_g^{1/2}$ range between 0.0 and 2.5). The inlet cooling water temperature is shown to have a significant effect on the flooding point except in the case of the smallest tube (see Fig. 9). For the other two tube sizes, the smaller the temperature gradient between the primary and the secondary side, the more the condensate film appears to be unstable, leading to a lower flooding point.

Figures 10–12 show that as the steam flow is increased to reach the flooding point (near point B in Fig. 10) a water column starts to build up during a short transient, to equilibrate the imposed pressure drop, resulting in an increased pressure in the bottom plenum. After the flooding point is reached, the trend in the experimental data shows no notable change in the condensation rates in terms of the Kutateladze variable 'K_g' as the pressure in the bottom plenum increases. This suggests that flooding at the tube inlet is the controlling process that causes the reflux condenser's capability of condensing steam to 'saturate'

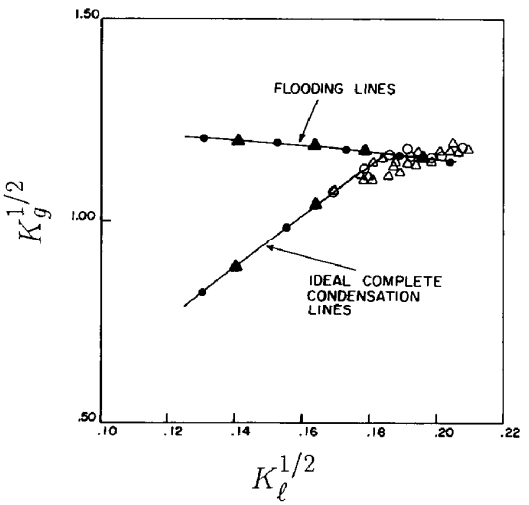

FIG. 9. Reflux condensation data in the $K_g^{1/2}$–$K_l^{1/2}$ plane for a 1.27 cm o.d. tube. (○) $T_{cw,i} = 18°C$; (△) $T_{cw,i} = 45°C$; (—●—) theory with $T_{cw,i} = 18°C$ and $f_{ie} = 0.0185$; (—▲—) theory with $T_{cw,i} = 45°C$ and $f_{ie} = 0.0185$.

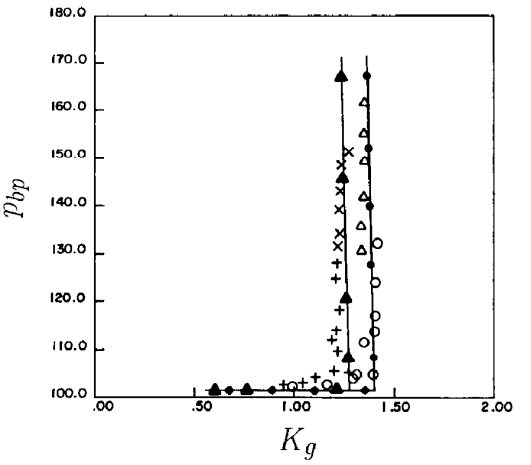

FIG. 11. Variations of the bottom plenum pressure as a function of steam flow rate for a 1.91 cm o.d. tube. (○) Upper plenum opened to atmosphere with $T_{cw,i} = 14°C$; (△) upper plenum pressurized with $T_{cw,i} = 14°C$; (+) opened to atmosphere with $T_{cw,i} = 45°C$; (×) upper plenum pressurized with $T_{cw,i} = 45°C$; (—●—) theory with $T_{cw,i} = 14°C$ and $f_{ie} = 0.0185$; (—▲—) theory with $T_{cw,i} = 45°C$ and $f_{ie} = 0.0227$.

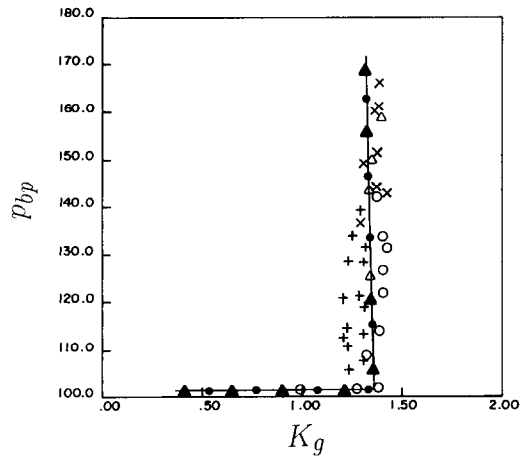

FIG. 12. Variations of the bottom plenum pressure as a function of steam flow rate for a 1.27 cm o.d. tube. (○) Upper plenum opened to atmosphere with $T_{cw,i} = 18°C$; (△) upper plenum pressurized with $T_{cw,i} = 18°C$; (+) opened to atmosphere with $T_{cw,i} = 45°C$; (×) upper plenum pressurized with $T_{cw,i} = 45°C$; (—●—) theory with $T_{cw,i} = 18°C$ and $f_{ie} = 0.0185$; (—▲—) theory with $T_{cw,i} = 45°C$ and $f_{ie} = 0.0227$.

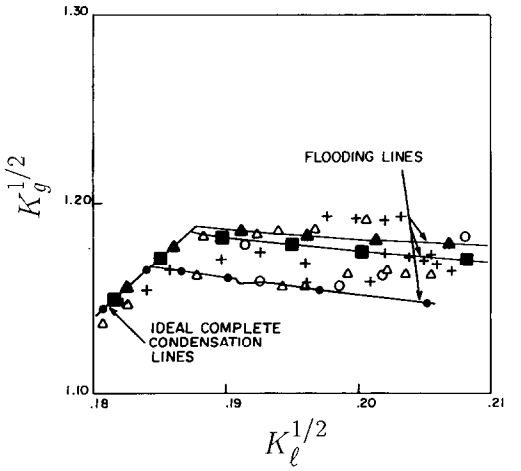

FIG. 13. Reflux condensation data in the $K_g^{1/2}$–$K_l^{1/2}$ plane for all tube sizes with the coldest cooling water temperature. (○) 1.27 cm o.d. tube with $T_{cw,i} = 18°C$; (△) 1.91 cm o.d. tube with $T_{cw,i} = 14°C$; (+) 2.54 cm o.d. tube with $T_{cw,i} = 10°C$; (—●—) theory for 1.27 cm o.d. tube, $T_{cw,i} = 18°C$ and $f_{ie} = 0.0185$; (—■—) theory for 1.27 cm o.d. tube, $T_{cw,i} = 18°C$ and $f_{ie} = 0.0185$; (—▲—) theory for 1.27 cm o.d. tube, $T_{cw,i} = 18°C$ and $f_{ie} = 0.0185$.

and it defines the maximum amount of steam flow that can be condensed in the total reflux condensation mode.

In the model of total reflux condensation given in the preceding section, the entrance interfacial friction factor f_{ie} is a free parameter that closes the set of equations. In general, the entrance condition influences the value of the parameter, which is usually greater than the correlation given for a position far from the entrance. Due to the complexity of the two-phase flow mechanics at the tube entrance, it is not possible yet to evaluate it by theoretical means and it must be evaluated empirically. As shown in Figs. 7–12, the present model fits the experimental data for the three tube sizes fairly well, with f_{ie} equal to 0.0185 for total reflux condensation and the lowest inlet cooling water temperature. In the case of total reflux condensation with the hottest cooling water temperature, the present model fits fairly well with the same value of the parameter f_{ie} equal to 0.0227, but for the smallest tube the original value of $f_{ie} = 0.0185$ had to be used. It can also be seen that in all the cases the present model fits the corresponding experimental data within the error of steam flow measurements ($\pm 5\%$) and it brings additional support to the assumptions made in the derivation of the present model.

For a given inlet cooling water temperature, the trends in the experimental data are not really affected by the variation of the tube diameter; however, the present model exhibits a small influence by the tube diameter on the flooding curve as illustrated in Fig. 13 for the lowest inlet cooling water temperature. The present model is seen to follow a behaviour where as the tube diameter is reduced the ordinate of the flooding curve decreases; this is similar to the behaviour of the Baharathan–Wallis model [15]. The results for the case of the hottest inlet cooling water temperature show the same behaviour but only for the two larger tubes, as depicted in Fig. 14. The behaviour of the model for the 1.27 cm o.d. tube can be explained by the choice of the value for the parameter f_{ie}. A close examination of Figs. 13 and 14 illustrates the fact that variations in both experimental and theoretical flow rates on the flooding curve, as a function of the tube diameter, are within the experimental error in the steam flow measurements. Therefore, it is concluded

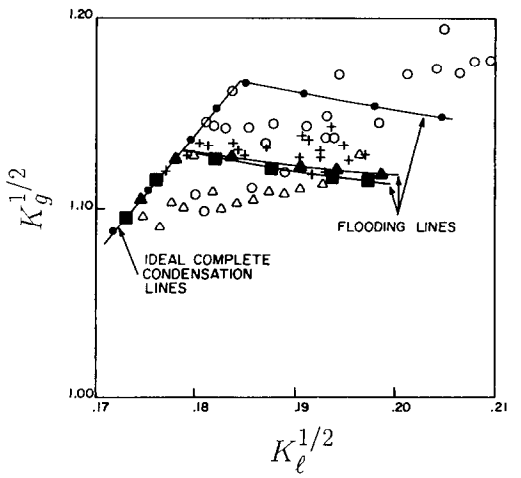

FIG. 14. Reflux condensation data in the $K_g^{1/2}$–$K_l^{1/2}$ plane for all tube sizes with the hottest cooling water temperature. (○) 1.27 cm o.d. tube with $T_{cw,i} = 45°C$; (△) 1.91 cm o.d. tube with $T_{cw,i} = 45°C$; (+) 2.54 cm o.d. tube with $T_{cw,i} = 45°C$; (—●—) theory for 1.27 cm o.d. tube, $T_{cw,i} = 45°C$ and $f_{ie} = 0.0185$; (—■—) theory for 1.91 cm o.d. tube, $T_{cw,i} = 45°C$ and $f_{ie} = 0.0185$; (—▲—) theory for 2.54 cm o.d. tube, $T_{cw,i} = 45°C$ and $f_{ie} = 0.0227$.

Table 1. Measured and calculated single-phase region lengths for 2.54 cm o.d. tube, $T_{cw,i}$ equal to 10°C and the upper plenum pressurized

p_{bp}	p_{up}	L_{sp} (measured)	L_{sp} (calculated)
138.138	111.327	2.21	2.73
135.658	111.029	1.97	2.51
129.325	111.193	1.28	1.85
155.423	129.651	2.24	2.62
150.895	129.214	1.80	2.21
144.274	129.274	1.15	1.53
135.044	128.925	0.30	0.62
165.614	139.563	2.39	2.65
159.688	137.673	1.80	2.24
155.389	138.046	0.54	1.76

that the influence of the tube diameter on the definition of the experimental flooding curve in total reflux condensation, in terms of Kutateladze variables, is negligible for the range of tube diameters studied, which is representative of what is found in steam generators. For tubes with much larger diameters, for example a feeder pipe in a CANDU-PHWR, the relative importance of the weight of the liquid film, the viscous forces in the liquid and the interfacial shear stress may be different.

For total reflux condensation in a 2.54 cm o.d. tube with inlet cooling water at 10°C the theoretical results define the path 'ABC' in Figs. 7 and 9. The path follows the so-called 'ideal complete condensation line' (point A to point B) before reaching the flooding line (at point B) and following it (point B to point C). This global behaviour has similarities with the work of other investigators [24]. This path can be considered as the response of the reflux condenser in terms of condensation rates to a variation in imposed pressure drops across the tube. The fairly good agreement between the present model and the experiment gives support to the postulate presented in Section 3.3 where the model is capable of predicting the global behaviour of the system in terms of condensation rates.

4.2. *Liquid hold-up*

One important question can be raised on the effects of flooding and tube length on the condensate distribution in the tube. The obvious answer is the appearance of a single-phase region oscillating over a two-phase region (see Fig. 2). Besides the amount of heat removed, computed via the condensation rates, the model predicts the length of these single-phase regions that could represent a significant amount of inventory that is not available for core cooling. Typical results are presented in Table 1; other cases can be found elsewhere [8]. In all the cases, the model overpredicts the length of single-phase region which is acceptable, giving a conservative estimate of the inventory that could be trapped in steam generator tubes.

5. CONCLUSIONS

Total reflux condensation phenomena in single vertical tubes were studied experimentally from which a phenomenological model has been derived. The good prediction of measured rates of condensation by the present model shows that flooding occurs at the tube inlet and plays a key role in defining the maximum heat removal and the distribution of the condensate hold-up in the tube. For the present tube entrance conditions (square edge), representative of what is found in an actual steam generator, the flooding flow rate, in terms of non-dimensional Kutateladze variable 'K_g', is not a function of tube diameter or the system pressure for the ranges of tube diameter and pressure studied. The inlet cooling water temperature has a notable influence on the definition of the flooding flow rate, for the hottest cooling water flooding occurs at a lower point than for the coldest water. The present model overpredicts the measured heat removal; however, that quantity can be obtained from the predicted condensation rates. A significant amount of condensate can be trapped in the tube in the form of a single-phase region. The agreement between the experimental data and the present model is satisfactory as the model overpredicts the single-phase region length, which is conservative from a reactor safety point of view.

The improved understanding developed in the present study of the mechanisms governing heat removal and liquid hold-up in total reflux condensation in vertical tubes is reflected in the good agreement between the experimental data and the present model in regard to the condensation rate and liquid hold-up. In steam generators, the cold and hot legs of the tube bundle can be considered as a bank of parallel vertical tubes. Different U-tube lengths and tube-to-tube interactions could well lead to instabilities such that total reflux condensation could not be maintained and transition to natural circulation could occur [1, 4, 5]. This could result in a situation where some tubes would experience natural circulation and others total reflux condensation. That situation would not correspond to the conservative case as the heat removal in natural circulation is in general greater than in total reflux condensation. The results of the present work could be used in a small-break LOCA analysis where the present model could estimate the heat removal capabilities (via the condensation rates) and the amount of coolant trapped in the steam generators, if, to be conservative, total reflux condensation is the assumed flow regime in each tube of the steam generators.

For the range of tube diameters studied, pertinent to steam generators, the present model could be applied as follows:

(i) given the geometry of a tube (l/D) and the proper boundary conditions (pressure drop across the tube and wall heat flux), the base flow characteristics

are computed for a given inlet steam mass flow rate '$\dot{m}_i$' using the extended Nusselt theory (see equations (6), (15), (21), (22) and (23)) plus global mass and energy balances;

(ii) equations (38) and (39) are solved simultaneously to find the minimum friction velocity at which the wave amplification factor is positive, giving the flooding steam flow rate '$\dot{m}_{fl}$' for the given base flow characteristics;

(iii) this flooding flow rate is compared to the given inlet steam flow rate; if it is greater, the inlet steam flow rate is increased in steps of $\Delta\dot{m}_i$ until an interval is defined where at the lower limit of the interval $\dot{m}_i < \dot{m}_{fl}$ and the upper limit of the interval $\dot{m}_i > \dot{m}_{fl}$; the flooding flow rate equating the inlet steam flow rate is then found by applying the method of bisection with a tolerance of 0.1%;

(iv) this flooding flow rate will be equal to the condensation rate by the assumption that total reflux condensation is the heat transfer mechanism; the heat removal is computed by multiplying the condensation flow rate by the latent heat corresponding to the bottom plenum pressure;

(v) the amount of coolant trapped in the single-phase region is calculated from the knowledge of the pressure drop in the two-phase region (see equation (23)) which is subtracted from the pressure drop across the tube yielding the pressure drop in the single-phase region; that pressure drop is due to gravity and the amount of coolant trapped is obtained by multiplying Δp_{sp} by the ratio of the tube cross-sectional area and the gravitational constant;

(vi) a conservative estimate for the total heat removed and the amount of coolant trapped in a given bank of vertical tubes is obtained by multiplying the above two quantities derived for a single tube by the total number of tubes.

Acknowledgements—The authors wish to express their appreciation to S. Banerjee for valuable suggestions, discussion and comments. This work was supported by Ontario-Hydro, the Natural Sciences and Engineering Research Council of Canada and the Ministère de l'Éducation du Québec.

REFERENCES

1. S. Banerjee, J. S. Chang, R. Girard and V. S. Krishnan, Reflux condensation and transition to natural circulation in a vertical U-tube, *ASME J. Heat Transfer* **103,** 719–727 (1983).
2. N. E. Burchill, Physical phenomena of small-break loss-of-coolant accident in a PWR, *Nuclear Safety* **23,** 525–536 (1982).
3. K. G. English, W. T. Jones, R. C. Speller and V. Orr, Criteria of flooding and flooding correlation studies with a vertical updraft partial condenser, *Chem. Engng Prog.* **59,** 51–53 (1963).
4. C. Calia and P. Griffith, *Modes of Circulation in an Inverted U-Tube Array with Condensation*, HTD—Vol. 15. ASME, New York (1981).
5. Q. T. Nugyen and S. Banerjee, Flow regimes and heat removal mechanisms in a single inverted U-tube steam condenser, *ANS Trans.* **43,** 788–789 (1982).
6. M. H. Chun and J. W. Park, Reflux condensation phenomena in vertical U-tubes with and without non-condensible gases, ASME Paper No. 84-WA/HT-2 (1984).
7. C. M. B. Russell, Condensation of steam in a long reflux tube, Research Symposium Paper No. HTFS RS 352 (1980).
8. R. Girard, Reflux condensation phenomena in single vertical tubes, Ph.D. Thesis, McMaster University (1985).
9. A. G. Cetinbudaklar and G. J. Jameson, The mechanism of flooding in vertical counter-current two-phase flow, *Chem. Engng Sci.* **24,** 1669–1680 (1969).
10. W. Nusselt, Ore Oberflachenkondensation des Wasserdamfes, *Z. Ver. Deustch. Ing.* **60,** 541, 569 (1916).
11. L. C. Burmeister, *Convective Heat Transfer*, p. 360. John Wiley, New York (1983).
12. H. R. Jacobs, An integral treatment of combined body force and forced convection in laminar film condensation, *Int. J. Heat Mass Transfer* **9,** 637–648 (1966).
13. W. M. Rohsenow, Heat transfer and temperature distribution in laminar film condensation, *Trans. ASME* **78,** 1645–1648 (1956).
14. B. Spindler, J. N. Solesio and J. M. Delhaye, On the equation describing the instability of liquid films with interfacial phase change. In *Two-phase Momentum Heat and Mass Transfer in Chemical, Process and Energy Engineering Systems* (Edited by F. Durat *et al.*), Vol. III. Hemisphere, Washington (1979).
15. D. Baharathan and G. B. Wallis, Air–water counter-current annular flow, *Int. J. Multiphase Flow* **9,** 349–366 (1983).
16. C. L. Tien, T. Fukano, K. Hijikata and S. J. Chen, Reflux condensation and operating limits of counter-current vapor liquid flows in closed tube, EPRI Report No. NP-2698 (1982).
17. T. Fujii, H. Uehare and K. Oda, Film-wise condensation on a surface with uniform heat flux and body force convection, *Heat Transfer Res. Japan* **1,** 76–83 (1972).
18. G. F. Hewitt and N. S. Hall-Taylor, *Annular Two-phase Flow*, p. 59. Pergamon Press, Oxford (1970).
19. B. Spindler, Equations gouvernant l'écoulement plan d'un film liquide avec flux de chaleur de la paroi et changement de phase à l'interface, Commissariat à l'Énergie Atomique, CAE-R-5061 (1981).
20. H. Schlichting, *Boundary Layer Theory*, pp. 438–442. McGraw-Hill, New York (1968).
21. M. Ünsal and W. C. Thomas, Linearized stability analysis of film condensation, *ASME J. Heat Transfer* **100,** 629–634 (1978).
22. B. E. Anshus and S. L. Goren, A method of getting approximate solutions to the Orr–Sommerfeld equation for flow on a vertical wall, *A.I.Ch.E. Jl* **12,** 1004–1008 (1966).
23. M. J. D. Powell, A FORTRAN subroutine for solving systems of non-linear algebraic equations, AERE-R-5847 (1968).
24. B. K.-H. Sun, M. Toren and S. Oh, Reflux condensation in a vertical channel flow, *Proc. 2nd Int. Topical Meeting on Nuclear Reactor Thermal-Hydraulics*, Santa Barbara (1983).

APPENDIX

Expressions for the variables in equations (35) *and* (36)

$$\beta_1 = \left[-\bar{k}^2 - \frac{i\bar{k}Re_0}{2}(\bar{u}_{fi}^{(0)} - \bar{c}^{(0)}) + \left(-i\bar{k}Re_0 \frac{\partial^2 \bar{u}_f^{(0)}}{\partial \bar{y}^2} - \frac{\bar{k}^2 Re_0^2}{4}(\bar{u}_{fi}^{(0)} - \bar{c}^{(0)})^2 \right)^{1/2} \right]^{1/2}$$

$$\beta_2 = \left[-\bar{k}^2 - \frac{i\bar{k}Re_0}{2}(\bar{u}_{li}^{(0)} - \bar{c}^{(0)}) - \left(-i\bar{k}Re_0 \frac{\partial^2 \bar{u}_l^{(0)}}{\partial \bar{y}^2} - \frac{\bar{k}^2 Re_0^2}{4}(\bar{u}_{li}^{(0)} - \bar{c}^{(0)})^2 \right)^{1/2} \right]^{1/2}$$

$$\beta_3 = -\bar{k}^2 - i\bar{k}Pe(\bar{u}_{li}^{(0)} - \bar{c}^{(0)})$$

$$L_1 = i\bar{k}Pe \frac{\partial \bar{T}_l^{(0)}}{\partial \bar{y}}$$

$$N_1 = \beta_1^2 + \bar{k}^2 + i\bar{k}Pe(\bar{u}_{li}^{(0)} - \bar{c}^{(0)})$$

$$N_2 = \beta_2^2 + \bar{k}^2 + i\bar{k}Pe(\bar{u}_{li}^{(0)} - \bar{c}^{(0)}).$$

Expressions for variables in the determinant of Fig. 5

$$\hat{c} = (\bar{u}_{li}^{(0)} - \bar{c}^{(0)})$$

$$b_{10} = -\beta_1^2 \cos\beta_1 + \beta_2^2 \cos\beta_2$$

$$b_{11} = \cos\beta_1 - \cos\beta_2$$

$$b_{12} = \sin\beta_1 - \frac{\beta_1}{\beta_2}\sin\beta_2$$

$$b_{13} = \frac{\cos\beta_1}{N_1} - \frac{\cos\beta_2}{N_2}$$

$$b_{20} = \beta_1^2 \sin\beta_1 - \frac{\beta_2^3}{\beta_1}\sin\beta_1$$

$$b_{21} = -\sin\beta_1 + \frac{\beta_2}{\beta_1}\sin\beta_2$$

$$b_{22} = -\frac{\sin\beta_1}{N_1} + \frac{\beta_2}{\beta_1}\frac{\sin\beta_2}{N_2}$$

$$c_{10} = -\beta_1 \sin\beta_1 + \beta_2 \sin\beta_2$$

$$c_{20} = -\beta_1 \cos\beta_1 + \frac{\beta_2^2}{\beta_1}\cos\beta_2$$

$$d_{10} = \frac{\sin\beta_1}{N_1} - \frac{\beta_1}{\beta_2}\frac{\sin\beta_2}{N_2}$$

$$a_1 = \frac{i}{\bar{k}}\frac{Ku}{Pe}\frac{\partial \bar{T}_l^{(0)}}{\partial \bar{y}}$$

$$a_2 = \frac{\partial \bar{T}_l^{(0)}}{\partial \bar{y}}$$

$$a_4 = -E$$

$$a_5 = \frac{i}{\bar{k}}\frac{Ku}{Pe}E$$

$$a_6 = 2\bar{k}\frac{(1-\gamma)}{\gamma}\frac{Ku^2}{Re_0 Pr^2}\frac{\partial \bar{T}_l^{(0)}}{\partial \bar{y}}$$

$$a_7 = \frac{i}{\bar{k}}\frac{Ku}{Pe}.$$

Expressions for the variables in equation (37)

$$D_1 = -\bar{k}Re_0\hat{c} - (3\bar{k}^2 + \beta_1^2)i$$

$$D_2 = -\bar{k}Re_0\hat{c} - (3\bar{k}^2 + \beta_2^2)i$$

$$E = \bar{k}P_s - \bar{k}^3 WeRe_0 - 2\bar{k}^3 \frac{M_r}{\gamma}\frac{Ku}{Pe}\frac{\partial \bar{T}_l^{(0)}}{\partial \bar{y}}$$

$$G_1 = \left(T_s - \frac{\partial^2 \bar{u}_l^{(0)}}{\partial^2 \bar{y}}\right) + \hat{c}(\bar{k}^2 - \beta_1^2)$$

$$G_2 = \left(T_s - \frac{\partial^2 \bar{u}_l^{(0)}}{\partial^2 \bar{y}}\right) + \hat{c}(\bar{k}^2 - \beta_2^2)$$

$$F_{ht}^{(1)} = \left(T_s - \frac{\partial^2 \bar{u}_l^{(0)}}{\partial^2 \bar{y}}\right)\left\{\beta_1^2\beta_2\left(\frac{D_1}{N_2} - \frac{D_2}{N_1}\right) \times \left(\frac{\beta_2}{\beta_1}\sin\beta_2\cos\beta_1 - \sin\beta_1\cos\beta_2\right) + \beta_1\beta_2\beta_3\left[\left(\frac{D_1}{N_1} - \frac{D_2}{N_2}\right) - \left(\frac{D_2\beta_2}{N_1\beta_1} + \frac{D_1\beta_1}{N_2\beta_2}\right) \times \sin\beta_1\sin\beta_2 - \left(\frac{D_2}{N_1} - \frac{D_1}{N_2}\right)\cos\beta_1\cos\beta_2\right]\tan\beta_3\right\}$$

$$F_{ht}^{(2)} = \beta_1\beta_2\beta_3\left\{\beta_1\beta_2(D_1 + D_2)\sin\beta_1\sin\beta_2 + (\beta_1^2 D_2 + \beta_2^2 D_1)\cos\beta_1\cos\beta_2 - (\beta_1^2 D_1 + \beta_2^2 D_2) + \bar{k} \times \left[(D_1 + D_2)(1 - \cos\beta_1\cos\beta_2) - \left(\frac{D_1\beta_1}{\beta_2} + \frac{D_2\beta_2}{\beta_1}\right)\sin\beta_1\sin\beta_2\right]\right\}\tan\beta_3$$

$$F_{ht}^{(3)} = -\beta_1\beta_2\beta_3\left[\left(\frac{G_1}{N_1} + \frac{G_2}{N_2}\right) - \left(\frac{G_1}{N_1}\frac{\beta_2}{\beta_1} + \frac{G_2}{N_2}\frac{\beta_1}{\beta_2}\right)\sin\beta_1\sin\beta_2 - \left(\frac{G_2}{N_1} + \frac{G_1}{N_2}\right)\cos\beta_1\cos\beta_2\right]$$

$$F_{ht}^{(4)} = \beta_2\beta_3\left[\frac{G_2}{N_1}\sin\beta_1\cos\beta_2 + \frac{G_1}{N_2}\frac{\beta_1}{\beta_2}\sin\beta_2\cos\beta_1\right]\tan\beta_3$$

$$F_{ht}^{(5)} = \beta_1\beta_2[\beta_1(c_{20}b_{13} - c_{11}b_{22}) + \bar{k}^2(b_{11}b_{13} - b_{12}b_{22})] + \beta_1\beta_2\beta_3[\beta_1(c_{20}d_{10} - c_{10}b_{13}) + \bar{k}^2(d_{10}b_{11} - b_{12}b_{13})]\tan\beta_3$$

$$F_{ht}^{(6)} = \beta_1\beta_2\beta_3\hat{c}(c_{10}b_{11} - c_{20}b_{12}) \times \left[2\bar{k}\frac{(1-\gamma)}{\gamma}\frac{Ku^2}{Re_0 Pr^2}\frac{\partial \bar{T}_l^{(0)}}{\partial \bar{y}} + \frac{iRe_0}{Pe}\frac{\partial \bar{u}_l^{(0)}}{\partial \bar{y}}\right]\tan\beta_3$$

$$F_{ht}^{(7)} = \bar{k}\frac{\partial \bar{u}_l^{(0)}}{\partial \bar{y}}\left(T_s - \frac{\partial^2 \bar{u}_l^{(0)}}{\partial^2 \bar{y}}\right)[(b_{11}b_{13} - b_{12}b_{22}) + \beta_2\beta_3(b_{11}d_{10} - b_{12}b_{13})\tan\beta_3]$$

$$F_{ht}^{(8)} = \left\{-\beta_1\beta_2\left(\frac{1}{N_1} - \frac{1}{N_2}\right)\left(T_s - \frac{\partial^2 \bar{u}_l^{(0)}}{\partial^2 \bar{y}}\right) \times (D_1\beta_1\sin\beta_1 - D_2\beta_2\sin\beta_2) + 2i\bar{k}^2\frac{(1-\gamma)}{\gamma}\frac{Ku}{Pr}\frac{\partial \bar{T}_l^{(0)}}{\partial \bar{y}}(G_2\cos\beta_2 - G_1\cos\beta_2) - E[(\bar{k}^2 - \beta_2^2)\cos\beta_2 - (\bar{k}^2 - \beta_1^2)\cos\beta_1]\right\}\frac{1}{\cos\beta_3}.$$

PHENOMENES DE LA CONDENSATION AVEC REFLUX DANS DES TUBES VERTICAUX SIMPLES

Résumé—Les phénomènes de la condensation avec reflux dans des tubes verticaux simples avec un rapport l/D élevé sont l'objet de la présente étude expérimentale et théorique. La combinaison de la théorie classique de Nusselt modifiée et d'une analyse linéaire de la stabilité du film du condensat a été utilisée pour créer un modèle mathématique des phénomènes observés expérimentalement. Une comparaison entre ce modèle et les résultats expérimentaux est présentée et discutée. Cette comparaison révèle un accord satisfaisant entre le modèle et les données expérimentales. Ceci indique que le modèle pourrait être utiliser dans l'analyse d'accidents dans les réacteurs nucléaires pour calculer la capacité d'enlèvement de chaleur des générateurs de vapeur quand sur le côté tube de ceux-ci on suppose que le transfert de chaleur se fait par condensation avec reflux.

RÜCKFLUSSKONDENSATION IN SENKRECHTEN EINZELROHREN

Zusammenfassung—Die Phänomene der Rückflußkondensation in senkrechten Einzelrohren mit großen l/D-Verhältnissen werden experimentell und analytisch untersucht. Ausgehend von den experimentellen Beobachtungen erfolgt die phänomenologische Modellierung durch Verknüpfung einer Erweiterung der klassischen Nusselt' schen Theorie mit einer linearisierten Stabilitätsanalyse der Kondensatfilmströmung. Der Vergleich des Modells mit den entsprechenden Versuchsdaten wird vorgestellt und diskutiert. Die zufriedenstellende Übereinstimmung von Modell und Meßdaten zeigt, daß dieses Modell zur Abschätzung der Kühlleistung von U-Rohr-Dampferzeugern bei der Analyse von Kernreaktorunfällen dienen könnte, falls der Wärmetransport auf der Rohrseite durch vollständige Rückflußkondensation erfolgt.

КОНДЕНСАЦИЯ В ОДИНОЧНЫХ ВЕРТИКАЛЬНЫХ ТРУБАХ

Аннотация—Экспериментально и аналитически исследуется явление конденсации в одиночных вертикальных трубах с большими отношениями l/D. На основе экспериментальных наблюдений проводится феноменологическое моделирование посредством сочетания обобщенной классической теории Нуссельта и линеаризованного анализа устойчивости пленочного течения конденсата. Проводится сравнение результатов моделирования с соответствующими экспериментальными данными. Удовлетворительное согласие между ними показывает, что рассматриваемая модель может использоваться при анализе аварии на ядерном реакторе для оценки возможностей теплоотвода парогенератора с U-образными трубами в случае, когда предполагается, что теплоотвод со стороны труб осуществляется за счет конденсации.